Effect of crystal quality on twinning stress in Ni-Mn-Ga magnetic shape memory alloys

Denys Musiienko¹, Frans Nilsén¹, Andrew Armstrong^{1,2}, Michal Rameš¹, Petr Veřtát¹, Ross H. Colman³, Jaroslav Čapek¹, Peter Müllner², Oleg Heczko^{1,3}, Ladislav Straka^{1,*}

- ¹ FZU Institute of Physics of the Czech Academy of Sciences, Na Slovance 1999/2, 18221, Prague 8, Czechia
- ² Micron School of Materials Science and Engineering, Boise State University, Boise, ID, 83725, USA
- ³ Faculty of Mathematics and Physics, Charles University, Ke Karlovu 5, 12116 Prague, Czechia

Abstract

Low twinning stress (TS) is a pre-requisite for magnetic shape memory functionality in ferromagnetic martensites. We compare $Ni_{50}Mn_{28}Ga_{22}$ (nominal at.%) single crystals from four different producers to reveal the effect of crystal quality on the TS. Near the reverse martensite transformation, the TS is generally low, about 1 MPa, regardless of mosaicity of up to 1.7° and chemical composition deviations of up to 2 at.% of Mn. Pure type I and type II twin boundaries occur in crystals with smooth chemical composition gradients. The corresponding temperature dependences of TS follow universal linear trends with the slopes of -0.045 MPa/K for type I twins and -0.001 MPa/K for type II twins, enabling a very low TS down to 2 K for the latter. An intermediate slope of -0.023 MPa/K appears for mixed type I/ type II twin boundaries in a crystal with sharp local chemical deviations. We conclude that the crystal quality affects the magnitude of the TS indirectly, through its impact on the character of the twin boundaries. The effect is weak near the martensite transformation temperature and strong at low temperatures.

Keywords: magnetic shape memory; twinning stress; crystal mosaicity; microstructure; single crystal; Ni-Mn-Ga.

^{*}corresponding author email: ladislav.straka@fzu.cz

1. Introduction

A distinct characteristic of Ni-Mn-Ga Heusler alloys with twinned martensite structure is their extraordinarily low twinning stress [1–4]. In combination with the material's ferromagnetic character and a high magnetocrystalline anisotropy energy, this enables magnetically induced reorientation (MIR) of martensite resulting in a large magnetic-field-induced strain (MFIS) of up to 12% and related functional properties [5–8]. The other interesting feature is a sharp difference in twinning stress for type I and type II twins in five-layered modulated (10M) martensite of Ni-Mn-Ga. The twinning stress is about one order higher for type I twins, approx. 1 MPa, in contrast to the extremely low twinning stress of type II twins, which can be less than 0.1 MPa [2,9,10].

The twinning stress in magnetic shape memory alloys is usually understood as a stress needed to move an existing twin boundary (TB), and it does not include the stress needed for nucleation of twins [7,11–13]. It can be considered as consisting of two components,

$$\sigma_{TW} = \sigma_{TW}^I + \sigma_{TW}^D, \tag{1}$$

where σ_{TW}^{I} is an *intrinsic component*, related to the propagation of a single TB in a perfect crystal, and σ_{TW}^{D} is a *defect component* resulting from the interaction of the moving TB with various crystal defects, such as crystal mosaicity, impurities, cracks and other TBs [12–16]. The intrinsic component links directly to the twinning mechanisms and only this component is usually considered in theoretical models.

Wang and Schitoglu [17] found that Ni-Mn-Ga had the lowest twinning stress (3.5 MPa) compared to other shape memory alloys (20–129 MPa) in their theoretical calculation based on a Peierls-Nabarro model. Using an elastic continuum approach Seiner et al. [18,19] ascribed the different twinning stresses of type I and type II twins to the different hierarchical twin arrangement – crossing twins vs branched *a/b* twin laminate – in the vicinity of the moving twin interface. Branched laminate of *a/b* twins was experimentally observed in Ref. [20]. Müllner considered the motion of TBs through the nucleation and growth of disconnection loops [21]. They concluded that the difference in nucleation (gradual for type II vs discrete for type I twins) of twinning disconnection loops is the main cause of the difference in the twinning stresses. The calculated twinning stress was 0.33 MPa for type II twins and 4.7 MPa for type I twins. Predicted temperature dependences were in qualitative agreement with the experiment [21].

Although the theoretical studies endeavour to explain the low twinning stress in Ni-Mn-Ga and its temperature dependence, the available experimental data related to the temperature dependence are in disagreement, as illustrated in Fig. 1. In the most recent works, Straka et al. suggests nearly linear temperature dependences with different slopes for type I and type II twins in 10M martensite of Ni-Mn-Ga alloy without the intermartensite transformation [22,23]. Preceding reports do not specify the type of twins. Okamoto et al. demonstrated linear dependence with a different slope [24,25]. Heczko et al. presented an exponential-like temperature dependence of the twinning stress [26]. Soolshenko et al. demonstrated linear temperature dependence again with a different slope for the twinning stress in 10M martensite phase [27].

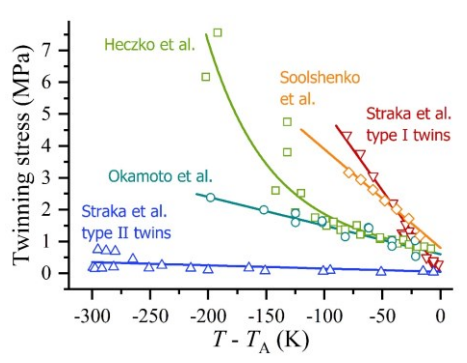


Figure 1. Temperature dependences of the twinning stress in 10M martensite of Ni-Mn-Ga reported by Straka et al. in Refs. [22,23] (triangles, only indicative measurement sets are shown for the sake of clarity), Okamoto et al. in Refs. [24,25] (circles), Heczko et al. in Ref. [26] (squares) and Soolshenko at al. in Ref. [27] (diamonds). Solid lines, curve and colours are provided for the guidance of the eye.

We can speculate that the differences in the previously reported temperature dependences of the twinning stress are related to the particular producer's methodology and the resulting crystal quality. A broader study comparing alloys from different producers with different preparative methods can provide a comprehensive explanation of the temperature dependences.

In this paper, we investigate how the crystal quality affects the twinning stress in 10M martensite single crystals of Ni-Mn-Ga. The crystals were obtained from four different sources to achieve a distinct scatter in chemical and crystalline homogeneity. For a comprehensive understanding we investigate the temperature dependences of the twinning stress and compare our results with the published data. Apart from the effort to explain the disagreement in the previous reports, an additional goal is to identify the effect of chemical inhomogeneity and mosaicity on the performance of magnetic shape memory single crystals in a wide temperature interval.

2. Materials and Methods

Single crystals, with a nominal composition of $Ni_{50}Mn_{28}Ga_{22}$, were grown in the MGML laboratory in Charles University, Czech Republic (CU), Boise State University, USA (BSU) and in the Institute of Physics of the Czech Academy of Sciences (FZU). The fourth crystal was obtained from the global material supplier Goodfellow Cambridge Ltd. (GF). At least two different growth methods were used: modified optical floating zone (CU and FZU with ingot diameter of 6 mm and 12 mm, respectively) and modified Bridgman (BSU) [9,28,29]. CU and FZU crystals were not heat-treated, the BSU crystal was homogenized at 1223 K for 48 h followed by a B2 \rightarrow L2₁ ordering treatment at 1023 K for 12 h. Production and heat-treatment methods for the GF crystal were not specified by the supplier.

The samples for measurements were cut by the producers into a shape of rectangular prisms with approximate faces orientation of $\{100\}_{\text{cubic}}$ in parent cubic austenite lattice cell basis. The average sample size was about $1\times2\times10~\text{mm}^3$, with the exception of the GF sample, used for mechanical testing, which had dimensions of $1.2\times5.2\times20~\text{mm}^3$, resulting from the originally obtained crystal sliced in half. The orientation of the longest edge of the CU, BSU and FZU samples was close to the growth direction of the single crystal ingots. The position of the GF sample inside the single crystal ingot was not specified by the supplier.

To remove any residual surface stresses, all the samples were electropolished at a temperature of 253 K using an electrolyte mixture of one part 60% HNO₃ and three parts denatured ethanol. Transformation temperatures, summarised in Table 1, were determined from the temperature-dependent low-field DC-magnetisation, measured using a vibrating sample magnetometer option of a Quantum Design PPMS. Martensite transformations occurred very sharply within a narrow temperature interval, similar to previous reports on single crystalline 10M martensite [30,31]. Differences between the start and end temperatures of martensite ($M_S - M_F$) and the end and start temperatures of reverse martensite ($A_F - A_S$) transformations were less than 4 K for all studied crystals. For the sake of clarity, we present the transformations only by the average transformation temperatures $T_M = (M_S + M_F)/2$ and $T_A = (A_S + A_F)/2$.

Table 1. Basic characteristics of the studied crystals: c/a ratio at room temperature, martensite transformation temperature, $T_{\rm M} = (M_{\rm S} + M_{\rm F})/2$, reverse martensite transformation temperature, $T_{\rm A} = (A_{\rm S} + A_{\rm F})/2$, Curie temperature, $T_{\rm C}$. Production methods are specified in footnotes.

Crystal name, year	c/a	$T_{\rm M}, { m K}$	T_{A} , K	$T_{\rm C}, { m K}$
CU ¹ , 2019	0.942	300	307	377
BSU ² , 2018	0.940	306	312	371
FZU1, 2019	0.937	316	324	372
GF ³ , 2019	0.939	310	321	375

¹ Modified optical floating zone, no heat-treatment.

Optical micrographs were taken with a Zeiss AxioImager.Z1 microscope. Stress-strain curves were measured using an in-house built compression device with a screw-based displacement control. The Honeywell FSG015WNPB force sensor with 15 N range assured higher accuracy in comparison to conventional mechanical testing machines with typically kN ranges. The twinning stress at room temperature was determined as the average level of the twinning plateau on the stress-strain curves.

Various physical and chemical parameters can be used to define the crystal quality [32–35]. Ni-Mn-Ga single crystals are known to exhibit high crystalline mosaicity and their physical properties highly depend on the chemical composition [36–38]. Thus, we define the crystal quality using chemical homogeneity and mosaicity criteria, evaluated from the chemical composition maps and the reciprocal space maps of the main diffraction peaks.

Chemical composition mapping was performed using an X-ray fluorescence (XRF) spectrometer, EDAX® AMETEK® ORBIS PC, equipped with a Rh anode tube ($E(K_\alpha) = 20.216 \; \text{keV}$) and Apollo XRF ML-50 EDS detector. The polycapillary focusing optics array was used to restrict the irradiated spot area to approx. $184 \times 69 \; \mu\text{m}^2$ (according to the factory calibration report) while maintaining high intensity. The samples were mounted on an XY-positioning table and measured whilst under vacuum. We estimate the absolute and relative measurement errors to be $\pm 0.5 \; \text{at.} \%$ and $\pm 0.1 \; \text{at.} \%$, respectively.

Lattice parameters were measured using a PANalytical X'Pert PRO diffractometer in line focus parallel beam geometry. A Co anode ($\lambda(K\alpha_1)=0.178901$ nm, $\lambda(K\alpha_2)=0.179290$ nm)

² Modified Bridgman, homogenization at 1223 K for 48 h followed by ordering at 1023 K for 12 h.

³ Production method was not specified.

was used as the X-ray source. The sample was attached to an ATC-3 texture cradle, enabling rotation, inclination and linear translation of the sample. Crystal mosaicity was determined from the 2θ - ω _{offset} maps by integrating the intensity over the 2θ axis. All crystal indices used hereafter refer to the martensite lattice with its coordinates inherited from the parent L2₁ lattice [2,39,40]. All the provided lattice constants relate to the average monoclinic structure, determined from the main diffraction peaks.

The temperature dependence of the twinning stress was determined from magnetisation loops following the procedure used in Refs. [23–25]. Magnetisation loops were measured at different temperatures by using a Cryogenic Ltd. vibrating sample magnetometer (VSM). To minimise the effect of demagnetisation, the samples were measured with their longest dimension parallel to the direction of the applied magnetic field. Only a single TB of a selected type was created and/or re-positioned to the middle of the sample prior to each measurement. The half of the sample that contained most of the visible defects (scratches, cracks) was reoriented into the magnetically preferable variant. During the measurement, the TB propagated through the other half of the sample [41].

MIR occurs at a certain magnetic field, called the switching field H_{SW} , which is seen on the magnetization loop as a distinct jump. At the switching field, the twinning stress, σ_{TW} , is equal to the magnetic driving force [42–44]:

$$\sigma_{TW} = \mu_0 M_S \left(H_{SW} - \left(\frac{M_S}{4K_U} \right) H_{SW}^2 \right) \frac{1}{\varepsilon_0}, \tag{2}$$

where $M_{\rm S}$ [A/m] is the saturation magnetisation, $K_{\rm U}$ [J/m³] is the magnetic anisotropy constant, $H_{\rm SW}$ [A/m] is the switching field and ε_0 is the tetragonal distortion of the lattice. $K_{\rm U}$ and $M_{\rm S}$, as functions of temperature, were determined from the separate measurements of magnetisation loops on single variant samples, similarly as in Refs. [23,24]. The tetragonal distortion was calculated as $\varepsilon_0 = 1 - c/a$, with c/a (Table 1) scaled in temperature according to the dependences published in Refs. [26,36]. Okamoto et al. [24,25] demonstrated that Eq. (2) provides reliable results that are close to the twinning stress measurements, determined by mechanical testing, even at low temperatures .

The twinning stress calculated from Eq. (2) is considered as the upper estimate as it does not include the effect of the demagnetisation field. The internal field in which the TB motion occurs is smaller than the measured external field. Consequently, the calculated σ_{TW} can be overestimated significantly especially for low H_{SW} observed for type II TB. The demagnetisation correction is complex and depends on the position of the TB [45] and thus is very difficult to include into experiment precisely. As such we did not take the demagnetisation field correction into account, which resulted in about +0.35 MPa stress level shift in comparison to the previous works, summarised in Fig. 1. The lack of correction, however, does not affect the temperature dependence of the σ_{TW} , since we can assume a small and constant demagnetization factor for the whole temperature interval.

3. Results and Discussion

3.1. Optical characterisation and twinning stress at room temperature

Various TBs can be created by repeated mechanical compressions and extensions of the samples in 10M martensitic phase at RT [46]. With sufficiently good single crystal quality, the material exhibits a tendency to nucleate a single or a few twin boundaries under the mechanical load. This is related to the large nucleation stress and simultaneous low twinning stress [4,7]. There is, however, no control of the TB type nucleated in a typical mechanical loading experiment, as the resolved shear stress is nearly identical for both type I and type II TBs. Practically, type I or type II TBs appear randomly in the single variant sample under a uniaxial load.

Here we employed the method proposed by Boiko et al. in Refs. [47,48] for TBs creation. The single variant state was achieved by a mechanical compression along the longest edge of the sample. A sharp-edged object (plastic prying tool and tweezers with plastic ends) was used to induce a shear stress perpendicularly to the short *c*-axis of the sample along the trace line of the desired TB. Then all but one TB were removed from the sample by applying stress locally in the near region of such TBs. The result of such procedure was a two variant sample with type I or type II TB with twinning elements and exact crystallographic orientations for 10M martensite described in detail previously [2,10,49]. For optical characterisation it is helpful that the surface traces of type I and type II TBs form a distinctive angle on the (100) face. For a typical {100} cut sample with <100> directions along sample axes the Type I TB trace is tilted 84° from sample edge while type I TB trace is exactly perpendicular to the sample edge, i.e. they form a 6° angle [2,9]. We derive the twin type from this angle.

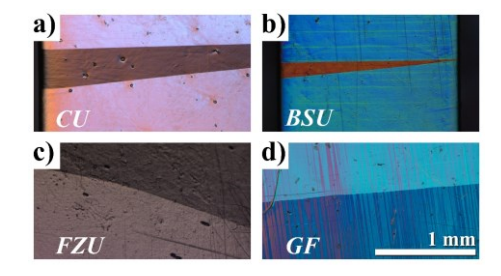


Figure 2. Optical micrographs of various TBs configurations formed in the studied samples.

Exemplary micrographs of the TBs for each sample are shown in Fig. 2, containing two boundaries (Fig. 2 a,b) or one boundary (Fig. 2 c,d), prepared by the method described above. The arrangement with two almost parallel TBs in the near proximity to each other (as in Fig. 2 a,b) was created for the purpose of illustration of TBs traces tilt. For the stress-strain measurements, arrangements with a single TB of particular type were preferred (as in Fig. 2 a,b)s. Two straight traces, one almost perpendicular to the sample edge (i.e. along [100]) and the other deviated by ~5° angle (i.e. deviated from [100], Fig. 2a, b) were ascribed to type I and type II TBs, respectively, in the CU and BSU samples [2,10]. Similar observations of two TB traces forming ~6° angle have been presented before for Adaptamat samples in Refs. [19,22]. It was not possible to create TBs with straight traces in the GF and FZU samples, which we initially ascribed to their inhomogeneity or other defects present in the crystal. The larger tilt of the TB trace in the FZU sample is caused by an approx. 8° deviation of the

Commented [RC1]: This is a little unclear due to wording. The earlier sentence describes the pairs of twin boundaries as just illustrative, referencing figure 2 a,b. But then this sentence says for the measurements you prefer a single TB of particular type, and also reference 2 a,b. I understand that a,b, is showing a single type, but figure c,d is showing a single boundary.

As you describe later that you were not able to create straight traces (single type), perhaps it's best to reference Fig 2 c,d rather than a,b above when talking about the prefered setup for measurement, just highlighting that it's a single TB.

Commented [RC2]: In the next section about the GF crystal you refer to this direction as [010]. Shouldn't this here also be [010]?

crystallographic orientation from the sample faces. Such a deviation changes the Schmidt factor by not more than 4%. Thus, the added error in the twinning stress measurement is small. Additional tilting of the TB is explained by the presence of a low-angle-deviated sub-grain.

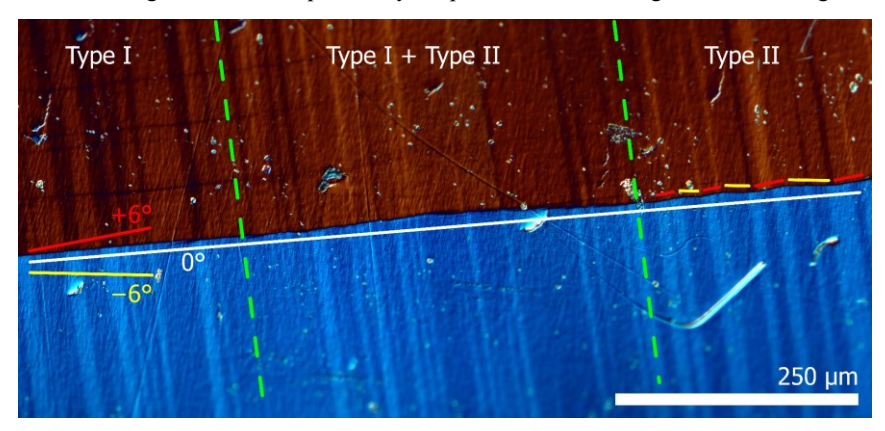


Figure 3. Optical micrograph of the twin boundary observed in the GF sample, Nomarski contrast. Dark and light stripes about perpendicular to the TB relate mainly to the "ghost" surface relief resulting from the sample polishing in the martensitic state. White line is parallel to type I TB segments. Red and yellow lines represent the deviation from this line by $+6^{\circ}$ and -6° , correspondingly. Green dashed lines are providing the guide for the eye, denoting the areas of type I and type II twins.

It was not possible to achieve a single variant state in the GF sample. We applied mechanical compressions and extensions repeatedly until a uniform twin structure was formed [50]. The resulting TB traces were never straight. They always consisted of many segments of various tilts, as shown in detail in Fig. 3. The segments, following closely [010] direction, were identified as traces of type I TB [18]. The white line in Fig. 3 is parallel to these segments. The segments that diverged by about $+6^{\circ}$ and -6° from this line constituted type II TB [18,20,49]. Additionally, there were discontinuities on the TB trace seen as a saw-like pattern with 0° and $\pm 6^{\circ}$ angles, which presumably appeared to accommodate the slight elastic incompatibility between the type I and type II parts of the boundaries. Such a mixture of type I and type II character of a TB was previously reported and its elastic compatibility was studied in Ref. [19].

An exemplary mechanical compression test with single type II TB motion in the BSU sample is presented in Fig. 4. Macrographs referring to the specific points on the stress-strain curve are shown as insets. The interactions of the TB with the cracks is observed here as narrow peaks on the stress-strain curve. The curve does not include the initial nucleation peak, since the TB was already present in the sample [7].

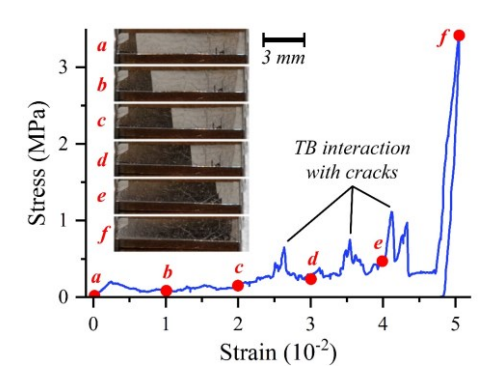


Figure 4. Example of the mechanical compression test performed for type II TB in the BSU sample. Video stills of the synchronised video footage at specific points on the stress-strain curve (marked by filled circles) are shown in the inset.

Representative stress-strain curves measured at RT for individual TBs with the specific tilt are shown in Fig. 5. There were clear stress plateaux observed in most experiments with distinctive high and low average plateau levels. The plateau levels were individually evaluated as the twinning stresses of the TBs. The latter parts of the curves (marked by grey rectangles in Fig. 5b, d) reflecting the interaction of the TB with the cracks on the sample edge were not taken into account.

In the CU and BSU samples, TBs nearly perpendicular to the sample edge exhibited higher twinning stress whereas inclined TBs showed lower twinning stress. Following the previous reports, Refs. [2,9,10,22], we ascribe the high stress levels (ranging from 0.5 to 0.8 MPa) of the plateaux observed for nearly straight TBs to type I while inclined TBs with low plateaux stress levels (\sim 0.1 MPa) we ascribe to type II TBs in the CU and BSU samples. The higher stress plateau at 0.5 MPa observed in the FZU sample is ascribed to type I TB. We observed that the type I TB trace in the FZU sample was curved (Fig. 5c), and we were not able to form a type II TB in this sample. This we ascribed to two factors: (1) a misorientation of the crystal by about 8° from the {100} planes; (2) the presence of a low angle grain boundary, almost parallel to the TB motion direction. The mixed type I / type II TBs in the GF sample showed the stress plateau at the level of 0.7 MPa.

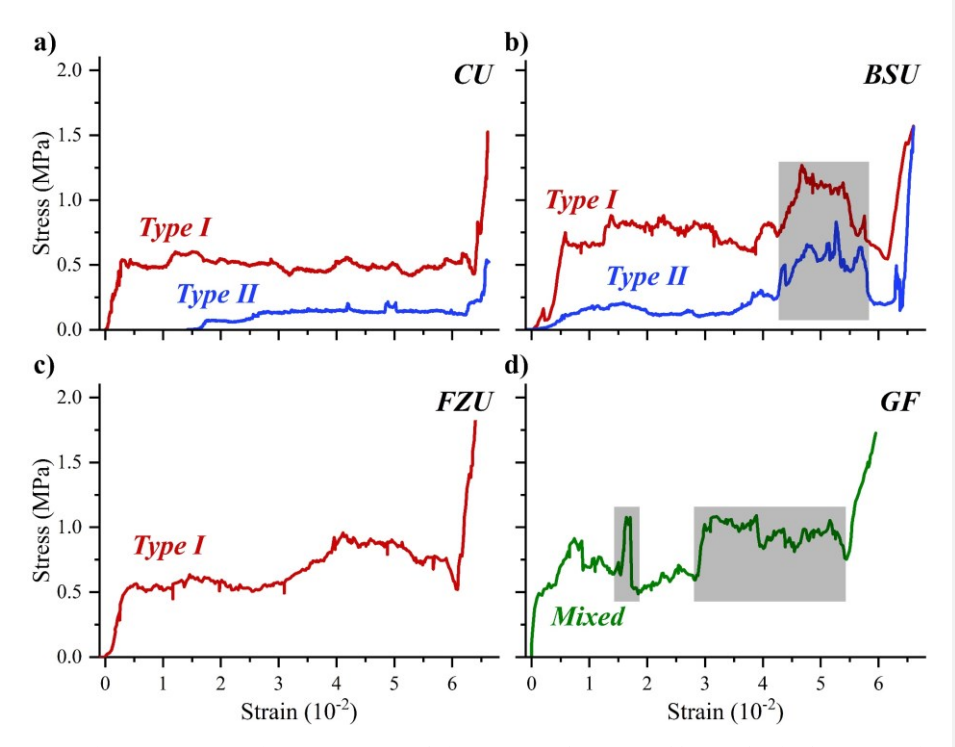


Figure 5. Stress-strain curves measured for type I (red), type II (blue) and mixed (green) twin boundaries in: (a) CU, (b) BSU, (c) FZU and (d) GF samples. Greyed areas of the plots mark the interaction of the moving twin boundary with cracks and other crystal defects.

Cracks were observed in all samples. The interaction of the moving twin boundary with the cracks increased the instant measured stress considerably. This was reflected as sharp upward steps and/or narrow peaks on the stress-strain curve, particularly in the latter part of the detwinning plateau preceding the elastic response (Fig. 4 and Fig. 5b, d, shaded areas). In terms of Eq. 1, we can say the defect component of the twinning stress increased significantly by the presence of cracks. To minimise this effect the affected parts of the plateaux were not considered for twinning stress evaluation.

3.2. Chemical homogeneity and crystalline mosaicity

Numerous parameters (e.g. porosity, degree of order, inclusions, vacancies, dislocation density etc.) can be linked to the crystal quality. For this study we selected chemical and crystalline homogeneities as two essential parameters related to crystal quality which were experimentally available and were expected to influence the twinning stress.

Chemical composition and homogeneity were determined using XRF area mapping. The chemical maps for Mn, which exhibited the largest variation for every crystal, are shown in Fig. 6. For the sake of clear comparison, the map area in figure was chosen to be the same for all samples $(2.7 \times 2.7 \text{ mm}^2)$. The measured area for the BSU sample (Fig. 6b) was limited by its width. The CU sample broke during additional experiments, not related to the present work, and the measured area was limited to the size of the recovered part.

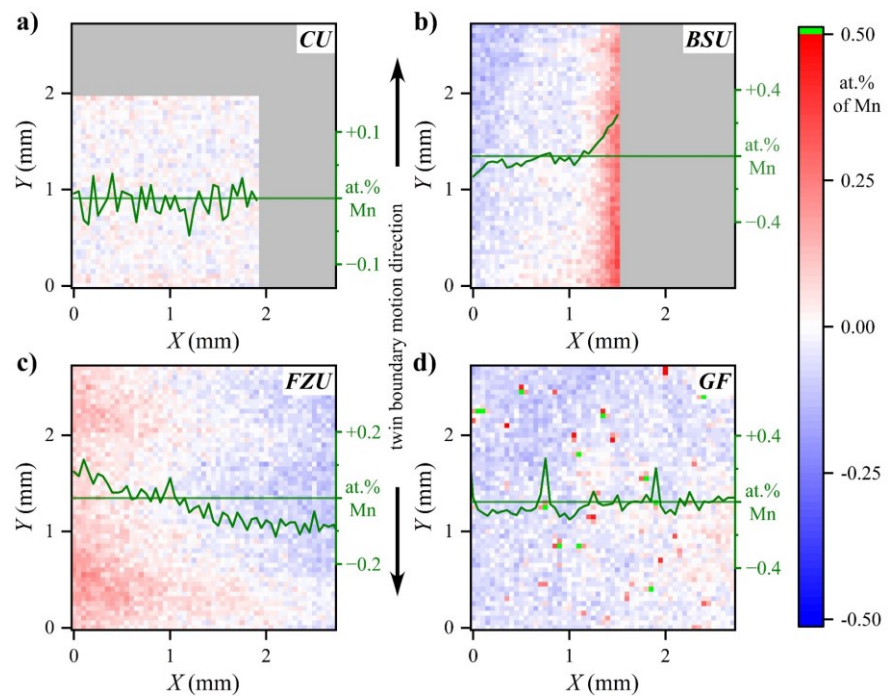


Figure 6. Chemical composition maps, measured by an X-ray fluorescence spectrometer, depicting the deviation of the manganese concentration from the average in (a) CU, (b) BSU, (c) FZU and (d) GF samples. Twin boundary motion direction during the mechanical and magnetic tests was parallel to the *ordinates* of the maps. Dark green curves represent line scans along the olive lines, averaged over three neighbouring measurement points. For CU and BSU samples (a, b), the maps are limited by the size of the samples. Light green points in (d) correspond to the deviation of measured manganese concentration between +0.5 and +2.1 at.%.

The chemical composition map of the CU sample (Fig. 6a) shows a very uniform composition distribution with variations within the instrumental error. In contrast, heat-treated BSU (Fig. 6b) and as-grown FZU (Fig. 6c) samples have moderate (about 0.5 at.% of Mn) composition gradient perpendicular to the TB motion direction. Despite this gradient, the samples exhibited twinning stresses comparable to the CU sample. Thus, we can conclude that moderate smooth composition gradient does not significantly affect the twinning stress.

The GF sample also exhibited moderate composition variation across the crystal (about 0.4 at.% of Mn). Moreover, it contained a number of sharp local composition fluctuations of more than 1 at.% of Mn (green dots in Fig. 6d). The latter can be explained by either true manganese concentration fluctuation or by impurities which can cause an apparent shift in the measured chemical composition. Notably, the density of these local defects was comparable to the scale of twin boundary segments observed within the TB of mixed type (Fig. 3). This suggests that the presence of such impurities is the primary reason for the formation of a mixed type I/ type II TB. It is known that variation in composition results in different lattice parameters or even a different martensite phase [36]. The significant local excess of Mn or local impurities are expected to generate substantial lattice stresses. These stresses may assist in nucleating twins and interact with the propagating TB, causing fragmentation of the TB into

multiple parts. The precise identification of the actual mechanism is beyond the scope of the present work.

It is known that Ni-Mn-Ga single crystals exhibit significant crystal mosaicity [10,29,51]. Crystal mosaicity was determined from 2θ - ω _{offset} maps for (400) / (040) reflections, see Fig. 7. The maps show splitting of the peaks both along the 2θ axis as well as along the ω _{offset} axis. The split along the 2θ axis is ascribed to (400) and (040) peaks resulting from the a-b laminate ({110} compound internal twins). This internal twinning near type I and type II TBs is nearly always present in 10M martensite and was described before theoretically in Refs. [10,18] as well as observed experimentally [20,38,49]. The laminate and TB can form so called crossing twins or the laminate can branch on the TB [10,20].

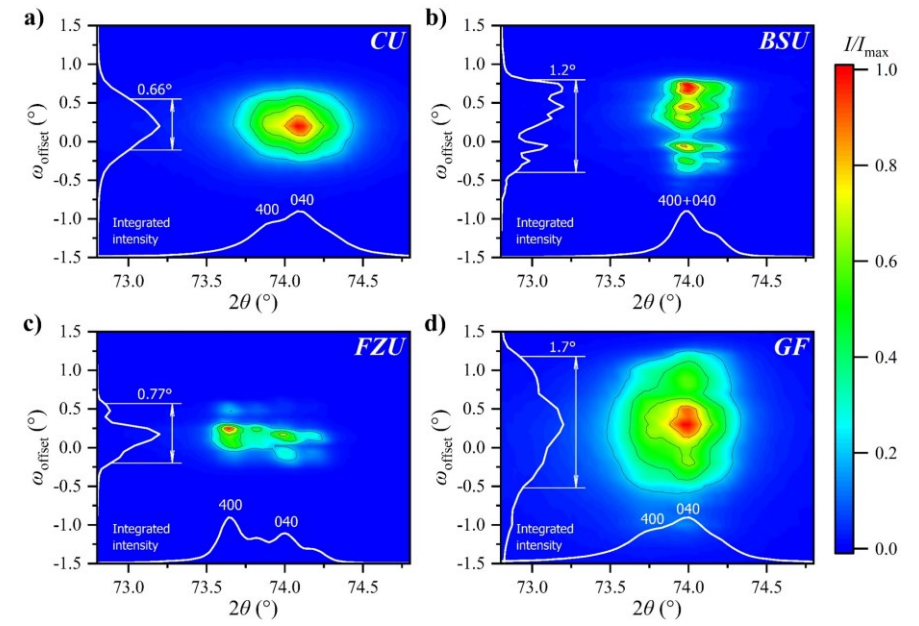


Figure 7. X-ray diffraction 2θ - ω _{offset} maps of (400) / (040) peaks for samples: (a) CU, (b) BSU, (c) FZU and (d) GF. Intensity is normalised for all the maps. Crystal mosaicity is determined from the graph of the integrated intensity as a function of ω _{offset} (left). Positions of (400) and (040) peaks are marked on the graph of the integrated intensity as a function of 2θ (bottom).

The distance between (400) and (040) peaks varied between crystals. This is explained by the variation in lattice parameters (see Table 2), which was in broad agreement with the compositional and temperature trends shown in Ref. [36]. The splitting of diffraction peaks along the ω_{offset} axis was present due to the crystal mosaicity. A drop of the intensity of the most distant peaks' tails to 50% was chosen as a criterion for mosaicity evaluation. Table 2 summarises chemical composition, lattice parameters and crystal mosaicity for all samples.

Table 2. Averaged composition, lattice parameters (in monoclinic approximation) and crystal mosaicity of the studied samples measured at room temperature.

Sample name	Ni, at. %	Mn, at. %	Ga, at. %	a, nm	b, nm	c, nm	γ	mosaicit y	
CU	50.1	27.5	22.4	0.5952	0.5938	0.5609	90.3°	0.66°	
BSU	51.9	25.3	22.8	0.5947	0.5944	0.5593	90.3°	1.20°	
FZU	50.0	28.1	21.9	0.5968	0.5944	0.5593	90.4°	0.77°	
GF	50.1	27.8	22.1	0.5962	0.5944	0.5597	90.3°	1.70°	

The largest mosaicity of 1.70° was observed in the GF crystal, followed by 1.20° in the BSU crystal, and the FZU and CU crystals having mosaicity of 0.77° and 0.66°, respectively. The large mosaicity may be the reason for our inability to form a pure type of TB in the GF crystal. In addition, the second highest mosaicity was exhibited by the BSU sample which had the highest twinning stress of pure type I TB. On the other hand, the CU and BSU samples had two times different mosaicity and exhibited very similar twinning stress for type II TBs (Fig. 5). Concerning the production methods, optical floating zone (CU, FZU) results in lower mosaicity in comparison to modified Bridgman (BSU).

3.3. Magnetisation measurements and twinning stress at low temperatures

Despite the difference in chemical and crystallographic imperfections the CU, BSU and FZU samples demonstrated similar mechanical behaviour for type I TBs at room temperature. Mixed type TBs in the GF sample exhibited twinning stress comparable to type I TBs in the CU, BSU and GF samples. Based on the previous works (Fig. 1) one can expect that much larger differences can be seen in the temperature dependences of the twinning stress. In this section we investigate the temperature dependence of the twinning stress, starting from the reverse martensite transformation temperature down to 2 K.

The twinning stress as a function of temperature was calculated from the temperature dependence of the switching field, determined from the measurements of magnetization loops. Exemplary magnetisation loops are shown in Fig. 8a with illustration of how $H_{\rm SW}$ was determined. The loops demonstrate all features typical for a single crystal exhibiting MIR, especially the typical first quadrant jump in magnetization and resulting first quadrant hysteresis [6,14,24]. The jump in magnetization at the switching field, $H_{\rm SW}$, is directly related to the occurrence of MIR. More specifically, in our case with only a single twin boundary initially present in the specimen, there is no nucleation barrier, and the twin boundary starts moving at the switching field [9,41]. The switching field as a function of temperature is depicted in Fig. 8b.

We calculated the twinning stress from H_{SW} using Eq. (2). The temperature dependence of the twinning stress is shown in Fig. 9. Following the suggestion in Ref. [22], that twinning stress depends on temperature relative to martensite transformation, the twinning stress is plotted as a function of relative temperature $T - T_A$, where T_A is the temperature of the reverse martensite transformation, see Table 1.

The twinning stress measurements, presented in Fig. 9, are limited to the 10M martensite phase and to temperatures below $T_{\rm A}$. The low-temperature limit for type I and mixed type I/type II twins is imposed by the rapid increase of twinning stress with decreasing temperature. The maximum twinning stress that can be determined by the used method is

limited by the maximum magnetic driving force developed in the studied crystals, which was found to be about 5 MPa for 10M martensite single crystals of Ni-Mn-Ga [26,52]. The twinning stress of type II twins grows very slowly with decreasing temperature. The low-temperature limit for type II twins is imposed by approaching an intermartensite transformation (IMT) [23,26,40]. Below some temperature, at which 10M martensite and the lower temperature phase are in thermodynamic equilibrium, the twinning stress of type II twins starts to increase [23]. We observed this behaviour in the BSU sample with measured IMT and reverse IMT temperatures of 73 K and 220 K, respectively. Just 1 K below the last measured point we did not detect any MIR indicating a very sharp dependence in agreement with the data shown in Ref. [23].

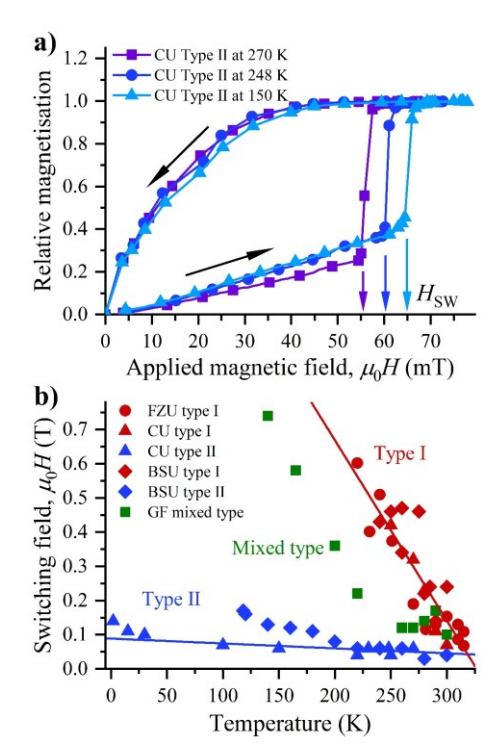


Figure 8. (a) Selected magnetisation loops for the CU sample at three different temperatures. Direction of the field sweep is indicated by black arrows. Determination of the switching field, H_{SW} , is illustrated by the coloured arrows. Difference in the initial magnetisation curve slopes is mainly caused by small variations in the twin boundary position and the sample location within the instrument. (b) Switching field, H_{SW} , as a function of temperature for type I (red), type II (blue) and mixed type I/ type II (green) twin boundaries. Solid lines are provided for eye guidance.

The CU sample showed no IMT in the measured temperature range and we were able to determine the temperature dependence for type II twins down to 2 K ($T - T_A = -305$ K). The twinning stress (upper estimate) was only 1.2 MPa at 2 K. The low twinning stress of type II twins approaching 0 K has previously been reported also for Adaptamat samples [53]. The

slight increase near 2 K can be attributed to either $T_{\rm IMT} \approx 0$ K [23] or to the role of thermal activation at low temperatures [21].

3.4. Generalized temperature dependences of the twinning stress

All crystals with pure TB types exhibited similar temperature dependences of the twinning stress, as depicted in Fig. 9. For type I twins the twinning stress increased linearly with decreasing temperature while for type II twins it was nearly temperature independent. The scatter in points was likely caused by multiple factors, such as a slight variation of the sample and initial TB positions during the measurements.

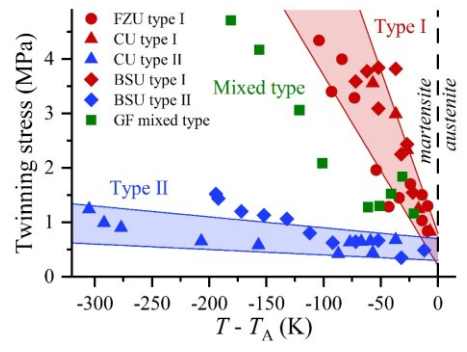


Figure 9. Calculated upper estimate for the twinning stress of type I (red), type II (blue) and mixed (green) twin boundaries. Solid lines and area fills are provided for the guidance of the eye.

Near the reverse martensite transformation, the twinning stress was about the same for both types of twins, as shown in Fig. 9. For type I twins it increased with decreasing temperature, with the slope of -0.045 MPa/K. The twinning stress of type II twins increased linearly with decreasing temperature, with the slope of -0.001 MPa/K. At low temperatures it increased faster, which was attributed to the IMT as discussed above.

The temperature dependences of the twinning stress, deduced from switching field measurements, for both pure type I and pure type II TBs were in broad agreement with the previous reports on Adaptamat samples [22,23,40,53], although our absolute values were about 0.4 MPa higher as demagnetization correction was not considered. Despite crossing the low angle grain boundary, type I TB in the FZU sample exhibited similar twinning stress as in the CU and the BSU samples. The temperature dependences of the twinning stress in CU, BSU, FZU and Adaptamat single crystals followed the same universal trends, marked by red and blue area shading in Fig. 9 for type I and type II TBs, respectively.

The observed universal trends indicate that the relatively large variation of the mosaicity in the studied crystals has only small effect on the twinning stress. In contrast, chemical inhomogeneity causes the formation of mixed type I / type II TB in the GF sample with altered temperature dependence of the twinning stress. This lays in-between the universal dependences for type I and type II TBs (Fig. 9), which suggests that the measured twinning stress is a superposition of the twinning stress values for type I and type II TBs. A linear fit gives the slope of -0.023 MPa/K for the temperature dependence of the twinning stress in the GF sample. On closer inspection, the dependence is initially flat, then rises at lower temperatures, meaning it can be alternatively seen as non-linear, exponent-like one. The intermediate character of the

dependence resembles the temperature dependences reported by Heczko at al. and Okamoto at al. in Refs. [24–26], Fig. 1. It can be inferred that the mixed type TBs were measured in these reports, which explains the significant deviations from the general trends for type I and type II twins.

The BSU and CU samples exhibit nearly the same twinning stress dependences despite the difference in composition of 2 at.% in Mn and 2 at.% in Ni, see Table 2. This indicates that 10M martensite structure always shows the same properties as a function of a relative temperature $(T-T_A)$, practically independent of composition. In other words, if a pure 10M martensite structure is established in a close to perfect crystal, the twinning stress dependences are expected to be universal and independent from the fluctuations in the chemical composition.

4. Conclusions

We compared Ni-Mn-Ga single crystals from four different producers to evaluate the effect of the crystal quality on the behaviour of twin boundaries. The variation in the crystal mosaicity in different crystals and moderate composition gradients across the samples had no significant effect on the twinning stress nor its temperature dependences, which followed the universal linear trends for type I and type II twins. In contrast, the mixed type I/ type II twin boundary, observed in the crystal with sharp local chemical defects and larger mosaicity, exhibited an intermediate slope of the twinning stress dependence, being relatively far from the universal trends for type I and type II twins.

We conclude that the crystal quality affects the magnitude of the twinning stress mainly indirectly, through its impact on the character of the twin boundaries. The resulting effect increases at low temperatures. If pure twin boundaries, either of type I or type II, can be created and maintained in the crystal, then they follow the respective universal trends in the temperature dependences of the twinning stress. However, for mixed type twin boundaries one can expect nearly arbitrary temperature dependences of the twinning stress, depending on the distribution of twin boundary types. They fall in between the temperature dependences of the twinning stress for type I and type II twins. The finding explains the notable disagreement between previous works that did not report the types of twins investigated. Mechanical discontinuities such as cracks always cause significant increase of the instant twinning stress in the respective part of the crystal, regardless of the twin boundary type.

From a functionality point of view, the modest chemical and crystalline inhomogeneities of 10M martensite single crystals of Ni-Mn-Ga have little to negligible effect on their twinning stress and expected magneto-mechanical response at room temperature near the martensitic transformation. However, use at lower temperatures may require higher control of chemical and crystallographic homogeneities for better regulation of the type of twins and the resulting twinning stress.

Acknowledgments

We acknowledge the support of Czech Science Foundation (grant No. 21-06613S) and of Operational Program Research, Development and Education financed by European Structural and Investment Funds and the Czech Ministry of Education, Youth and Sports (Projects SOLID21 - CZ.02.1.01/0.0/0.0/16_019/0000760, MATFUN - CZ.02.1.01/0.0/0.0/15_003/0000487 and International mobility MSCA-IF IV FZU - CZ.02.2.69/0.0/0.0/20_079/0017754). Part of the experiments was performed in MGML (http://mgml.eu), which is supported within the program of Czech Research Infrastructures (project no. LM2018096). PM acknowledges partial financial support through the National Science Foundation project DMR-1710640.

References

- [1] V.A. Chernenko, S. Besseghini, Ferromagnetic shape memory alloys: Scientific and applied aspects, Sensors Actuators, A Phys. 142 (2008) 542–548. https://doi.org/10.1016/j.sna.2007.05.023.
- [2] A. Sozinov, N. Lanska, A. Soroka, L. Straka, Highly mobile type II twin boundary in Ni-Mn-Ga five-layered martensite, Appl. Phys. Lett. 99 (2011) 124103. https://doi.org/10.1063/1.3640489.
- [3] M. Acet, L. Mañosa, A. Planes, Magnetic-Field-Induced Effects in Martensitic Heusler-Based Magnetic Shape Memory Alloys, in: Handb. Magn. Mater., Elsevier B.V., 2011: pp. 231–289. https://doi.org/10.1016/B978-0-444-53780-5.00004-1.
- [4] L. Straka, N. Lanska, K. Ullakko, A. Sozinov, Twin microstructure dependent mechanical response in Ni-Mn-Ga single crystals, Appl. Phys. Lett. 96 (2010). https://doi.org/10.1063/1.3373608.
- [5] A. Sozinov, N. Lanska, A. Soroka, W. Zou, 12% magnetic field-induced strain in Ni-Mn-Ga-based non-modulated martensite, Appl. Phys. Lett. 102 (2013) 021902. https://doi.org/10.1063/1.4775677.
- [6] A.A. Likhachev, K. Ullakko, Magnetic-field-controlled twin boundaries motion and giant magneto-mechanical effects in Ni-Mn-Ga shape memory alloy, Phys. Lett. Sect. A Gen. At. Solid State Phys. 275 (2000) 142–151. https://doi.org/10.1016/S0375-9601(00)00561-2.
- [7] I. Aaltio, O. Söderberg, Y. Ge, S.P. Hannula, Twin boundary nucleation and motion in Ni-Mn-Ga magnetic shape memory material with a low twinning stress, Scr. Mater. 62 (2010) 9–12. https://doi.org/10.1016/j.scriptamat.2009.09.012.
- [8] A.A. Likhachev, A. Sozinov, K. Ullakko, Modeling the strain response, magnetomechanical cycling under the external stress, work output and energy losses in Ni-Mn-Ga, Mech. Mater. 38 (2006) 551–563. https://doi.org/10.1016/j.mechmat.2005.05.022.
- [9] D. Kellis, A. Smith, K. Ullakko, P. Müllner, Oriented single crystals of Ni-Mn-Ga with very low switching field, J. Cryst. Growth. 359 (2012) 64–68. https://doi.org/10.1016/j.jcrysgro.2012.08.014.
- [10] L. Straka, O. Heczko, H. Seiner, N. Lanska, J. Drahokoupil, A. Soroka, S. Fähler, H.

- Hänninen, A. Sozinov, Highly mobile twinned interface in 10 M modulated Ni-Mn-Ga martensite: Analysis beyond the tetragonal approximation of lattice, Acta Mater. 59 (2011) 7450–7463. https://doi.org/10.1016/j.actamat.2011.09.020.
- [11] A.A. Likhachev, A. Sozinov, K. Ullakko, Influence of external stress on the reversibility of magnetic-field-controlled shape memory effect in Ni-Mn-Ga, in: C.S. Lynch (Ed.), Smart Struct. Mater. 2001 Act. Mater. Behav. Mech., 2001: p. 197. https://doi.org/10.1117/12.432757.
- [12] U. Gaitzsch, M. Pötschke, S. Roth, B. Rellinghaus, L. Schultz, A 1% magnetostrain in polycrystalline 5M Ni-Mn-Ga, Acta Mater. 57 (2009) 365–370. https://doi.org/10.1016/j.actamat.2008.09.017.
- [13] A.A. Likhachev, K. Ullakko, The model of magnetic-field-controlled shape memory effect in NiMnGa, J. Phys. IV JP. 11 (2001) Pr8-293-Pr8-298. https://doi.org/10.1051/jp4:2001850.
- [14] O. Heczko, A. Soroka, S.P. Hannula, Magnetic shape memory effect in thin foils, Appl. Phys. Lett. 93 (2008). https://doi.org/10.1063/1.2957675.
- [15] L. Straka, H. Hänninen, N. Lanska, A. Sozinov, Twin interaction and large magnetoelasticity in Ni-Mn-Ga single crystals, J. Appl. Phys. 109 (2011) 063504. https://doi.org/10.1063/1.3552292.
- [16] P. Müllner, G. Kostorz, Microstructure of magnetic shape-memory alloys: Between magnetoelasticity and magnetoplasticity, Mater. Sci. Forum. 583 (2008) 43–65. https://doi.org/10.4028/www.scientific.net/msf.583.43.
- [17] J. Wang, H. Sehitoglu, Twinning stress in shape memory alloys: Theory and experiments, Acta Mater. 61 (2013) 6790–6801. https://doi.org/10.1016/j.actamat.2013.07.053.
- [18] H. Seiner, L. Straka, O. Heczko, A microstructural model of motion of macro-twin interfaces in Ni-Mn-Ga 10 M martensite, J. Mech. Phys. Solids. 64 (2014) 198–211. https://doi.org/10.1016/j.jmps.2013.11.004.
- [19] O. Heczko, L. Straka, H. Seiner, Different microstructures of mobile twin boundaries in 10 M modulated Ni-Mn-Ga martensite, Acta Mater. 61 (2013) 622–631. https://doi.org/10.1016/j.actamat.2012.10.007.
- [20] O. Heczko, L. Klimša, J. Kopeček, Direct observation of a-b twin laminate in monoclinic five-layered martensite of Ni-Mn-Ga magnetic shape memory single crystal, Scr. Mater. 131 (2017) 76–79. https://doi.org/10.1016/j.scriptamat.2017.01.010.
- [21] P. Müllner, Twinning stress of type I and type II deformation twins, Acta Mater. 176 (2019) 211–219. https://doi.org/10.1016/j.actamat.2019.07.004.
- [22] L. Straka, A. Soroka, H. Seiner, H. Hänninen, A. Sozinov, Temperature dependence of twinning stress of Type I and Type II twins in 10M modulated Ni-Mn-Ga martensite, Scr. Mater. 67 (2012) 25–28. https://doi.org/10.1016/j.scriptamat.2012.03.012.
- [23] L. Straka, A. Sozinov, J. Drahokoupil, V. Kopecký, H. Hänninen, O. Heczko, Effect of intermartensite transformation on twinning stress in Ni-Mn-Ga 10 M martensite, J. Appl. Phys. 114 (2013). https://doi.org/10.1063/1.4817717.
- [24] N. Okamoto, T. Fukuda, T. Kakeshita, Magnetocrystalline anisotropy and twinning stress in Ni-Mn-Ga ferromagnetic shape memory alloys, in: J. Phys. Conf. Ser., Institute of Physics Publishing, 2006: pp. 315–318. https://doi.org/10.1088/1742-6596/51/1/073.
- [25] N. Okamoto, T. Fukuda, T. Kakeshita, Temperature dependence of rearrangement of martensite variants by magnetic field in 10M, 14M and 2M martensites of Ni-Mn-Ga alloys, Mater. Sci. Eng. A. 481–482 (2008) 306–309. https://doi.org/10.1016/j.msea.2006.12.218.
- [26] O. Heczko, L. Straka, Temperature dependence and temperature limits of magnetic shape memory effect, J. Appl. Phys. 94 (2003) 7139–7143.

- https://doi.org/10.1063/1.1626800.
- [27] V. Soolshenko, N. Lanska, K. Ullakko, Structure and twinning stress of martensites in non-stoichiometric Ni 2 MnGa single crystal, J. Phys. IV. 112 (2003) 947–950. https://doi.org/10.1051/jp4:20031037.
- [28] J. Wang, C. Jiang, Single-crystal growth of NiMnGa magnetic shape memory alloys, J. Cryst. Growth. 310 (2008) 865–869. https://doi.org/10.1016/j.jcrysgro.2007.11.197.
- [29] P. Cejpek, L. Straka, M. Veis, R. Colman, M. Dopita, V. Holý, O. Heczko, Rapid floating zone growth of Ni2MnGa single crystals exhibiting magnetic shape memory functionality, J. Alloys Compd. 775 (2019) 533–541. https://doi.org/10.1016/j.jallcom.2018.10.113.
- [30] A. Sozinov, A.A. Likhachev, K. Ullakko, Magnetic and magnetomechanical properties of Ni-Mn-Ga alloys with easy axis and easy plane of magnetization, in: C.S. Lynch (Ed.), Smart Struct. Mater. 2001 Act. Mater. Behav. Mech., SPIE, 2001: p. 189. https://doi.org/10.1117/12.432756.
- [31] M. Vronka, L. Straka, H. Seiner, M. Karlík, O. Heczko, Mechanical Stabilization of Martensite: Comparison of Ni-Mn-Ga and Cu-Ni-Al Shape Memory Single Crystals, 134 (2018). https://doi.org/10.12693/APhysPolA.134.627.
- [32] Z. Han, C. Wang, L. Shi, Synthesis and characterization of helium-charged titanium hydride films deposited by direct current magnetron sputtering with mixed gas, Mater. Des. 119 (2017) 180–187. https://doi.org/10.1016/j.matdes.2017.01.044.
- [33] D. Nakamura, I. Gunjishima, S. Yamaguchi, T. Ito, A. Okamoto, H. Kondo, S. Onda, K. Takatori, Ultrahigh-quality silicon carbide single crystals, Nature. 430 (2004) 1009–1012. https://doi.org/10.1038/nature02810.
- [34] H.H. Fang, R. Raissa, M. Abdu-Aguye, S. Adjokatse, G.R. Blake, J. Even, M.A. Loi, Photophysics of organic-inorganic hybrid lead iodide perovskite single crystals, Adv. Funct. Mater. 25 (2015) 2378–2385. https://doi.org/10.1002/adfm.201404421.
- [35] M. Li, Y. Cheng, T. Yu, J. Wu, J. He, N. Liu, T. Han, G. Zhang, Critical thickness of GaN film in controllable stress-induced self-separation for preparing native GaN substrates, Mater. Des. 180 (2019) 107985. https://doi.org/10.1016/j.matdes.2019.107985.
- [36] N. Lanska, O. Söderberg, A. Sozinov, Y. Ge, K. Ullakko, V.K. Lindroos, Composition and temperature dependence of the crystal structure of Ni-Mn-Ga alloys, J. Appl. Phys. 95 (2004) 8074–8078. https://doi.org/10.1063/1.1748860.
- [37] V. V. Martynov, V. V. Kokorin, The crystal structure of thermally- and stress-induced Martensites in Ni ₂ MnGa single crystals, J. Phys. III. 2 (1992) 739–749. https://doi.org/10.1051/jp3:1992155.
- [38] A. Saren, A. Sozinov, S. Kustov, K. Ullakko, Stress-induced a/b compound twins redistribution in 10M Ni-Mn-Ga martensite, Scr. Mater. 175 (2020) 11–15. https://doi.org/10.1016/j.scriptamat.2019.09.001.
- [39] L. Righi, F. Albertini, L. Pareti, A. Paoluzi, G. Calestani, Commensurate and incommensurate "5M" modulated crystal structures in Ni-Mn-Ga martensitic phases, Acta Mater. 55 (2007) 5237–5245. https://doi.org/10.1016/j.actamat.2007.05.040.
- [40] L. Straka, J. Drahokoupil, O. Pacherová, K. Fabiánová, V. Kopecký, H. Seiner, H. Hänninen, O. Heczko, The relation between lattice parameters and very low twinning stress in Ni50Mn25+xGa25-x magnetic shape memory alloys, Smart Mater. Struct. 25 (2016). https://doi.org/10.1088/0964-1726/25/2/025001.
- [41] L. Straka, H. Hänninen, O. Heczko, Temperature dependence of single twin boundary motion in Ni-Mn-Ga martensite, Appl. Phys. Lett. 98 (2011) 141902. https://doi.org/10.1063/1.3573860.
- [42] R.C. O'Handley, Model for strain and magnetization in magnetic shape-memory alloys,

- J. Appl. Phys. 83 (1998) 3263-3270. https://doi.org/10.1063/1.367094.
- [43] P. Müllner, V.A. Chernenko, M. Wollgarten, G. Kostorz, Large cyclic deformation of a Ni-Mn-Ga shape memory alloy induced by magnetic fields, J. Appl. Phys. 92 (2002) 6708–6713. https://doi.org/10.1063/1.1513875.
- [44] E. Faran, D. Shilo, Implications of twinning kinetics on the frequency response in NiMnGa actuators, Appl. Phys. Lett. 100 (2012) 151901. https://doi.org/10.1063/1.3702459.
- [45] O. Heczko, D. Vokoun, V. Kopecky, M. Beleggia, Effect of magnetostatic interactions on twin boundary motion in NiMnGa magnetic shape memory alloy, IEEE Magn. Lett. 6 (2015). https://doi.org/10.1109/LMAG.2015.2449252.
- [46] A. Mizrahi, D. Shilo, E. Faran, Variability of Twin Boundary Velocities in 10M Ni– Mn–Ga Measured Under μ s -Scale Force Pulses, Shape Mem. Superelasticity. 6 (2020) 45–53. https://doi.org/10.1007/s40830-020-00264-4.
- [47] Boiko V.S., Garber R.I., Determination of the Phenomenological Dislocation Theory Parameters for Elastic Twins in Calcite, Sov. Phys. J. Exp. Theor. Phys. 23 (1966) 602. http://www.jetp.ac.ru/cgi-bin/e/index/r/50/4/p905?a=list.
- [48] A.M. Kosevich, V.S. Boĭko, Dislocation theory of the elastic twinning of crystals, Sov. Phys. Uspekhi. 14 (1971) 286–316. https://doi.org/10.1070/PU1971v014n03ABEH004704.
- [49] R. Chulist, L. Straka, N. Lanska, A. Soroka, A. Sozinov, W. Skrotzki, Characterization of mobile type I and type II twin boundaries in 10M modulated Ni-Mn-Ga martensite by electron backscatter diffraction, Acta Mater. 61 (2013) 1913–1920. https://doi.org/10.1016/j.actamat.2012.12.012.
- [50] M. Chmielus, V.A. Chernenko, W.B. Knowlton, G. Kostorz, P. Müllner, Training, constraints, and high-cycle magneto-mechanical properties of Ni-Mn-Ga magnetic shape-memory alloys, in: Eur. Phys. J. Spec. Top., Springer-Verlag, 2008: pp. 79–85. https://doi.org/10.1140/epjst/e2008-00657-3.
- [51] A. Sharma, S. Mohan, S. Suwas, Evidence of adaptive modulation and magnetic field induced reorientation of variants in epitaxially grown Ni-Mn-Ga thin film on Al2O3 (112⁻0) substrate, Mater. Sci. Eng. B Solid-State Mater. Adv. Technol. 242 (2019) 6– 16. https://doi.org/10.1016/j.mseb.2019.02.015.
- [52] H.E. Karaca, I. Karaman, B. Basaran, Y.I. Chumlyakov, H.J. Maier, Magnetic field and stress induced martensite reorientation in NiMnGa ferromagnetic shape memory alloy single crystals, Acta Mater. 54 (2006) 233–245. https://doi.org/10.1016/j.actamat.2005.09.004.
- [53] O. Heczko, V. Kopecký, A. Sozinov, L. Straka, Magnetic shape memory effect at 1.7 K, Appl. Phys. Lett. 103 (2013). https://doi.org/10.1063/1.4817941.